

Collective motion and solid-liquid-type transitions in vibrated granular layers

Nicolás Mujica and Francisco Melo

*Departamento de Física de la Universidad de Santiago de Chile,
Av. Ecuador 3493, Casilla 307 Correo 2 Santiago-Chile*

From pressure and surface dilation measurements, we show that a solid-liquid-type transition occurs at low excitation frequencies in vertically vibrated granular layers. This transition precedes subharmonic bifurcations from flat surface to standing wave patterns, indicating that these waves are in fact associated with the fluid like behavior of the layer. In the limit of high excitation frequencies, we show that a new kind of subharmonic waves can be distinguished. These waves do not involve any lateral transfer of grains within the layer and correspond to excitations for which the layer slightly bends alternately in time and space. These bending waves have very low amplitude and we observe them in a vibrated two-dimensional layer of photoelastic particles.

I. INTRODUCTION

In a driven granular system, such as a vibrated layer composed of macroscopic particles, energy is dissipated by inelastic grains collisions and by friction. Also, for realistic situations, the typical energy of a grain is many orders of magnitude greater than $k_B T$, so the temperature does not play an important role in the dynamics of these materials. However, it is commonly observed that granular matter behaves like solids, liquids or even gases depending on the energy injection and energy dissipation rates [1]. More precisely, the competition between these quantities determines the residual velocity fluctuations which in turn play the role of thermal fluctuations in these materials. From this view point, surface waves excited by vertical vibrations provide one of the most striking examples in which granular materials act like a fluid. For a granular layer, it was well established that parametric waves can be observed whenever the dimensionless acceleration $\Gamma = A(2\pi f)^2/g$ exceeds a critical value [2] (here g is the acceleration of gravity, A is the amplitude of the vibrating surface, and f is the frequency of the driving force). The primary instability resulted from a flat layer to a pattern of squares or stripes, depending on both f and the particle diameter, d . As an illustration we present two typical snapshots of these kind of waves in Fig. 1 a and b. It was found that the crossover frequency f_d at which the square to stripe transition occurs is proportional to $d^{-1/2}$. In addition, this scaling was qualitatively understood in terms of the ratio of kinetic energy injected into the layer to the potential energy required to raise a particle a fraction of its diameter. At low f , the horizontal mobility should be high since the layer dilation is large [3,4], whereas at large f , the mobility should be low since layer dilation is small [5]. We notice, however, that these waves are the corresponding hydrodynamic surface modes of the layer since they require a transfer of mass to be sustained [2,4,5].

In this paper, we report on measurements of the pres-

sure due to the layer-container collision and the surface and bulk dilation of the layer. We show that there exists a critical Γ for which the flat layer undergoes a phase transition. This critical Γ is smaller than the critical one at which waves appear. At low f this transition is a solid-liquid type, at intermediate f only a heating up of the surface layer is observed, whereas at high f a compaction transition is detected. Thus, our results show that granular surface waves are naturally linked to the fluid like behavior since they are observed only when the energy input per particle is enough to induce a minimal dilation of the flat layer. At high f and for the same critical value of Γ at which hydrodynamic waves appear, bending waves are detected instead. In this regime, our measurements show that the mobility of grains is almost completely suppressed in both the bulk and the free surface of the layer. In this case, a set of experiments conducted with large photoelastic particles allow us to observe these waves as an alternation of bright and dark zones that oscillate in time at half of the forcing frequency. In addition, we show for the low frequency regime that when Γ is increased to a value close to 4.6, an inverse transition from a fluid to a compact layer is observed. This transition is responsible for the flat with kinks state reported in previous works [2] (See Fig. 1 c and d). A brief summary of our results has been given in ref. [5].

This article is organized as follows: section II is devoted to the description of our experimental setup. In section III, which is the main part of this article, we present our pressure measurements and we establish the basis to obtain density profiles and the bulk dilation from the experimental data. In section IV we present surface dilation measurements and we discuss how they link to the bulk dilation measurements. The energy dissipation rate in the vibrated layer is also estimated as a function of the excitation frequency. Section V is concerned with the study of the very low amplitude regime of surface waves and its connection with the compact state of the layer. Finally a brief discussion is given.

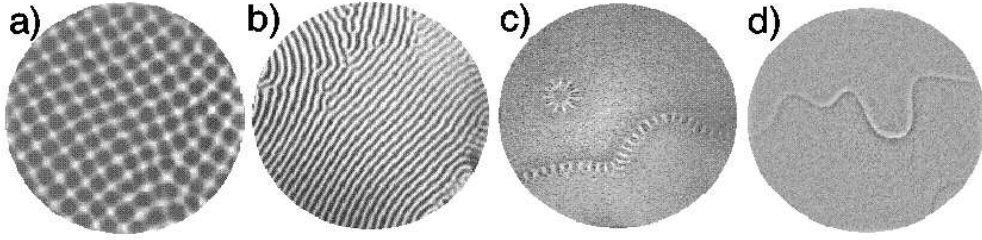


FIG. 1. Snapshots of the layer state at different conditions obtained in a large cell. a) Squares, $f \sim 20$ Hz, $\Gamma = 3.0$. b) Stripes, $f \sim 60$ Hz, $\Gamma = 3.0$. c) Flat with kinks at $f \sim 25$ Hz, $\Gamma = 4.7$. d) Flat with kinks at $f \sim 60$ Hz, $\Gamma = 4.7$.

II. EXPERIMENTAL SETUP

In this article we present two sets of experiments. In the first set, we measure simultaneously the pressure resulting from the collisions of the layer with the vibrating plate and the surface particle dilation. From the pressure measurements, we obtain information on the bulk dilation and density (see section III). The surface dilation is determined through the normalized reflected intensity of the surface layer (See discussion below).

In fig. 2 we present a schematic drawing of the experimental setup. In this experiment, a thin layer of $0.106 - 0.125$ mm diameter bronze particles, 15 particles deep, is placed at the bottom of a 40 mm diameter and 25 mm height cylindrical container. The container's wall is Lucite while the base is aluminum to reduce electrostatic effects. The container is mounted on a high frequency response pressure sensor (PCB. Model 208A11) which is driven by an electromechanical vibration exciter. The resulting acceleration is measured to a resolution of $0.01g$. A second Lucite cylinder is used as a lid for the whole system allowing evacuation of the container to less than 0.1 Torr; at this value volumetric effects of the gas are negligible [6]. The surface of the layer is illuminated at low angle (20° respect to the horizontal) by an array of 18 LEDs organized in a 10 cm diameter ring. The reflected light from the surface layer is focused by a lens of 28 mm focal length on a flat photodiode of 25 mm^2 area. The whole system is automatically run by a Power PC computer equipped with A/D and GPIB boards.

With this set-up, the measured light is proportional to both the incident light and the reflectivity coefficient of the bronze particles R ($R \sim 0.6$). We notice that only a small fraction s , which is about 5 percent of the surface of a single particle, reflects light in the direction of the solid angle of the camera (in the experiment, lens aperture angle is about 12°). The intensity I , measured by the photodiode, can be then taken proportional to the surface density or more precisely to the number of particles within the first layer. Furthermore, I relates to surface dilation δ_s as $I/I_0 \approx d^2/(d + \delta_s)^2$, where I_0 is a reference intensity for which we take $\delta_s = 0$ [7]. We neglect multiple reflections, since their dominant contribution is proportional to both R^2 and s^2 , where s^2 represents the probability of having a secondary reflection within the

solid angle of the camera. Thus, by taking the incident light in a small enough angle, we insure that, to a first approximation, only the first layer of particles contribute to I .

The second set of experiments consists of vibrating a two dimensional layer of photoelastic particles and taking images of the layer motion with a high speed CCD camera. The goal is to observe the very low amplitude waves found in the high frequency regime. A cell made of two glass plates 400 mm wide by 100 mm high was mounted on the moving platform of our vibrator system. The gap between the plates is controlled by spacers of varying thickness to a resolution of 0.05 mm. Images with resolution of 256×256 pixels are captured at rates of 1200 frames per second by a Hisis 2002 CCD camera. Images are obtained by transmission using parallel light with incidence perpendicular to the cell. Transmitted light is filtered through a polarizer whose axis is perpendicular to direction of polarization of the incident light. More details are given in section V.

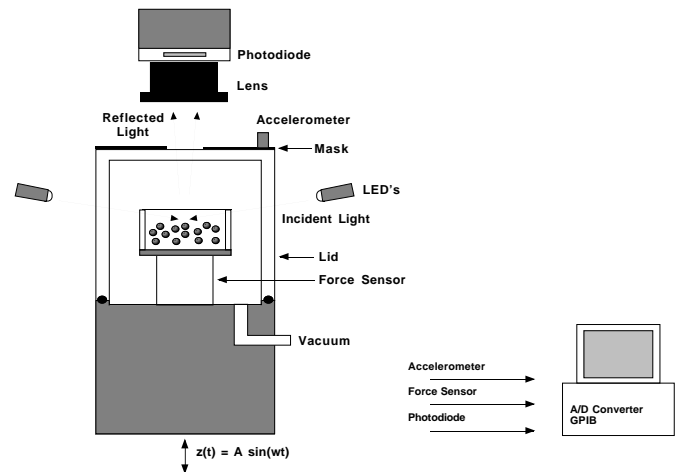


FIG. 2. A schematic drawing of the apparatus showing the cylindrical cell, the location of the pressure sensor, and the setup for reflectivity measurements.

III. PRESSURE MEASUREMENTS AND DENSITY PROFILES

A. Experimental procedures and collision model

In Fig. 3a, we present a typical pressure signal $P(t)$ as a function of time for $f = 40$ Hz and $\Gamma = 2.2$. This signal is composed of a sinusoidal component, corresponding to the force required to accelerate the cell, and of a peak sequence, due to the layer-plate collisions. We are interested in the shape of the peak during the collision so it is necessary to subtract the sinusoidal component. By this procedure we obtain a number of pressure peaks, typically about 15. As an illustration, we show in Fig. 3b the average peak obtained from the peaks presented in Fig. 3a. To characterize the peaks of a sequence like the one presented we take the maximum value P and the width T_c , which is a measure of the collision time. More precisely these quantities are obtained as the averages of the sequence $\{P^{(k)}, T_c^{(k)}\}$, where k is an integer that indicates the collision number, i.e. $P = \langle P^{(k)} \rangle$ and $T_c = \langle T_c^{(k)} \rangle$ where $\langle \rangle$ denotes the sequence average. For the data in the Fig. 3, $P = 2.45 \pm 0.03$ kPa and $T_c = 0.52 \pm 0.01$ ms (In this case T_c is taken as the width at a pressure equal to a quarter of P).

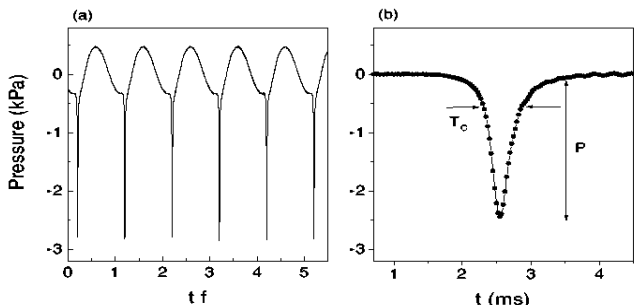


FIG. 3. (a) Time evolution of the pressure signal $P(t)$ for $f = 40$ Hz and $\Gamma = 2.2$. In (b) we present the averaged collision peak obtained from $P(t)$, and we show the definition of the maximum pressure P . The collision time T_c is the width of the peak at certain height.

Now, due to the impulsive nature of the layer plate collision, we write the following scaling relation

$$P \sim \frac{M V_c}{A_p T_c} \quad (1)$$

where M is the total mass of the layer, A_p is the active surface of the plate and V_c is the layer-plate relative velocity at the collision. If the collision takes place at time $t = \bar{t}$ and is completely inelastic then $V_c = V_p(\bar{t}) - V_b(\bar{t})$, where V_p and V_b are the plate and layer velocity respectively. Thus, in practice, we approximate the collision velocity by the one predicted by the completely inelastic ball model. We note that this model assumes that the

layer losses immediately all its energy and takes the velocity of the moving plate. This approximation is valid since previous experiments have shown, by measuring the flight time of the layer, that the motion of the center of mass of the layer follows the motion of an inelastic ball [2,8].

We remark that in our experiments, even close to $\Gamma \sim 1$, the vertical average bulk dilation of the layer, δ_b , is never strictly zero. This is concluded because the collision time is not determined by the Hertz theory. Indeed, experiments performed by E. Falcon *et al* [9] have shown that, in the case of a column of N particles in contact ($\delta_b = 0$) colliding vertically with a fixed plate, the collision time is $T_c = (N-1)T_q + \tau_1$, where N is the number of particles, T_q is the time duration of the momentum transfer from one particle to another, and τ_1 is the collision time between two particles predicted by Hertz theory [10]. Now, for the particles used in our experiments the orders of magnitude of these times are $T_q \approx \tau_1 \approx 10^{-6}$ s [11]. Then, the predicted collision time for our three dimensional layer should be of order $T_c \approx 10^{-5}$ s. This order of magnitude is never observed in our experiments, where for Γ close to 1 and for a wide range of f the minimum collision time is of order $T_c \approx 5 \times 10^{-4}$ s. The difference between what is expected from the Hertz prediction for $\delta_b = 0$ and the experimental values for T_c can be explained if the layer is slightly dilated at the collision; a local dilation of 1 percent ($\delta_b/d \sim 0.01$) drastically changes the collision regime from Hertz contact to ballistic collisions. Although this effect has interesting consequences on sound propagation, it does not affect the center of mass motion of the layer. Thus, for $\Gamma > 1$ we write the total dilation of the layer as $\Delta = V_c T_c$. If in addition we assume that dilation is homogeneous, i.e. $\Delta = N \delta_b$, where N is the number of layers, we can write equation (1) as

$$P \sim \frac{M V_c^2}{A_p N \delta_b} \quad (2)$$

Thus, our procedure to measure the local bulk dilation δ_b is: we fit P versus V_c/T_c to obtain the numerical factor of equation (1) and we then use equation (2) to obtain the value of δ_b .

In the following, we will relate the layer density to the pressure signal $P(t)$. Fig. 4 presents a schematic view of a collision. We consider that the plate collides with the granular layer of density $\rho(z)$ at a velocity V_c at time $t = 0$. Then, the layer is initially fixed in space and the plane $(x, y, z = 0)$ of the reference frame (x, y, z) coincides with the inferior layer just before the collision (See Fig. 4a). We also notice that the mass of the plate M_p is much larger than the mass M of the layer ($M/M_p \sim 0.01$) so we neglect any velocity change of the plate due to momentum transfer. We also neglect the variation of the relative velocity due to the action of gravity since experimentally we observe that $gT_c \ll V_c$. Thus, the force exerted on the plate due to de momentum transfer is

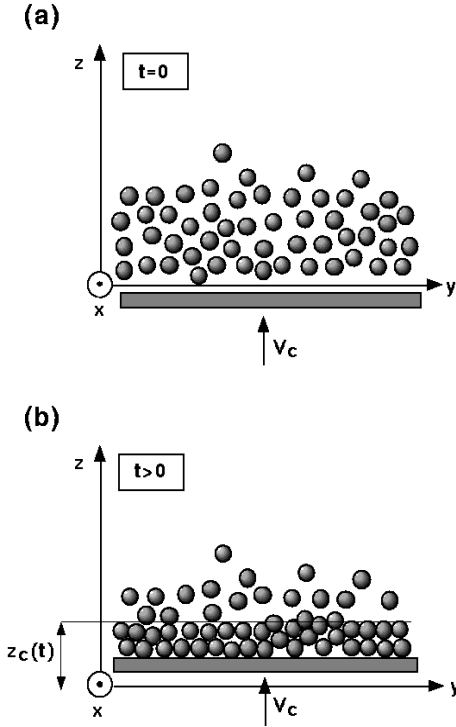


FIG. 4. Schematic of the collision. Fig. (a) shows the instant $t = 0$ at which the plate collides with the layer. The velocity of the collision is V_c and the density of the layer before the collision is $\rho(z)$; Fig. (b) shows how the layer accumulates over the moving plate at an instant $t > 0$. We also present the definition of $z_c(t)$ as the position of the compression front relative to the origin of the fixed frame (x, y, z) . In all the calculations the effect of gravity is neglected, since experimentally $gT_c \ll V_c$.

$$F(t) \approx \frac{dm(t)}{dt} V_c \quad (3)$$

Here $m(t)$ is the mass that has collided with the plate at time t . In the next we need to link $dm(t)/dt$ to $\rho(z)$, measured in the fixed frame (x, y, z) . To do this we define the compression front $z_c(t)$ as the height (relative to the fixed frame) of the mass that has been deposited on the plate at time t (see Fig. 4b). So, the mass $m(t)$ accumulated on the plate becomes

$$m(t) = A_p \int_0^{z_c(t)} \rho(z) dz \quad (4)$$

whose derivative with respect to time is

$$\frac{dm(t)}{dt} = A_p \rho(z_c(t)) \frac{dz_c(t)}{dt} \quad (5)$$

Now, at time t the plate has moved a distance $V_c t$ from its initial position, and the height of the layer with respect to the plate can be written

$$h(t) \equiv \frac{m(t)}{A_p \rho_o} = \frac{1}{\rho_o} \int_0^{z_c(t)} \rho(z) dz \quad (6)$$

where ρ_o is the density of the layer in the compact state. We then obtain

$$z_c(t) = V_c t + \frac{1}{\rho_o} \int_0^{z_c(t)} \rho(z) dz \quad (7)$$

Differentiating this equation respect to time, we obtain the density evaluated at the location of the compression front as a function of its velocity $\dot{z}_c(t)$

$$\rho(z_c(t)) = \rho_o \left(1 - \frac{V_c}{\dot{z}_c(t)} \right) \quad (8)$$

Using this result in equation (5), the relation (3) for the force becomes

$$\frac{F(t)}{A_p \rho_o V_c} = \dot{z}_c(t) - V_c \quad (9)$$

Integrating this equation between 0 and t gives us an expression for the compression front as a function of time

$$z_c(t) = V_c t + \frac{1}{A_p \rho_o V_c} \int_0^t F(\bar{t}) d\bar{t} \quad (10)$$

In summary, from the pressure signal $P(t) = F(t)/A_p$ we deduce the time evolution of the compression front $z_c(t)$. Also, we use equation (8), which tells us about the time evolution of density at the compression front. Since the time t enters as a simple parameter we can obtain the density as a function of z_c , right before the collision.

Finally, we notice that both equations (8) and (9) are laws for the conservation of mass and momentum through the compression front. It is possible to deduce from them the velocity of the compression front and the pressure in the compressed part of the layer as implicit functions of $\rho(z_c(t))$,

$$\begin{aligned} \dot{z}_c(t) &= \frac{\rho_o V_c}{\rho_o - \rho(z_c(t))} \\ \frac{F(t)}{A_b} &= \frac{\rho_o \rho(z_c(t)) V_c^2}{\rho_o - \rho(z_c(t))} \end{aligned}$$

These expressions are generalizations of those obtained by Goldshtein *et al* [12] for the propagation of a shock wave through an homogeneous layer of inelastic particles.

Before presenting our experimental results we will show that with equation (10) we can check the momentum conservation of the collision. Evaluating it at time $t = T_c$ (here T_c is the total collision time) we obtain

$$z_c(T_c) = V_c T_c + \frac{1}{A_p \rho_o V_c} \int_0^{T_c} F(\bar{t}) d\bar{t} \quad (11)$$

Since by definition $z_c(T_c) = H + V_c T_c$, where H is the layer thickness in the compact state and $V_c T_c$ is the total displacement of the plate during the collision, and $\rho_o = M/H A_p$, we find

$$\int_0^{T_c} F(\bar{t}) d\bar{t} = M V_c \quad (12)$$

B. Experimental results

We begin this section by presenting results concerning the momentum conservation relation (12). Experimentally we have checked it for a wide range of parameters, namely $1 < \Gamma < \Gamma_w \approx 2.8$ and $35 \text{ Hz} < f < 350 \text{ Hz}$. The main point is that, in our experiment, the velocity V_c calculated from the completely inelastic ball model is a very good approximation. As the internal degrees of freedom of the layer are excited one expects that this approximation becomes less accurate. However, this only occurs in the wave regime where the take off velocity is reduced and then both the collision velocity and the flight time are smaller than predicted [2].

There are other experimental effects that should be considered. For instance, friction on the cell walls can transfer momentum to the layer. Another possibility, much less probable, is the transfer of momentum to the walls by the formation of dynamical arcs. Therefore, we expect that the correct form of the momentum conservation, taking into account all possible sources of errors, to be

$$\int_0^{T_c} F(\bar{t}) d\bar{t} = M_{eff} V_c \quad (13)$$

where M_{eff} is an effective mass, and V_c is the velocity of collision calculated from the completely inelastic ball model. From this model, we know that $V_c = gF(\Gamma)/f$, where $F(\Gamma)$ is a nonanalytic function of Γ , which is found numerically [8]. From our data we find then that the scaling $\int_0^{T_c} F(\bar{t}) d\bar{t} \sim V_c$ is very well verified as a function of both Γ and f . As expected, we find that M_{eff} is independent of both Γ and f and is slightly lower than M .

In order to complete our description, it is necessary to estimate the granular density in the compact state ρ_o . This quantity is in principle a dynamical variable, in the sense that it depends on how we compact our layer. However, we notice that the important parameter in (10) is $A_p \rho_o = M/H$. Taking in to account the previous discussion about the effective mass of the layer and that $H \approx 1.7 \text{ mm}$, we obtain $A_p \rho_o \approx 4.2 \text{ kg/m}$.

Fig. 5 presents averaged pressure peaks for several values of Γ at $f = 40 \text{ Hz}$. Each curve is obtained by averaging 15 collisions, in the same way as that for the one presented in Fig. 3b. We notice that our analysis is valid for cases for which $\Gamma < \Gamma_w$, where $\Gamma_w \approx 2.8$ is the onset for parametric waves. Thus, the last pressure curve presented for $\Gamma = 2.98$ is shown to display the difference of the parametric wave state; at this value of Γ the collision is quite spread out in time and the maximum pressure achieved is also much smaller. We will discuss more this point in the next section. For the other pressure curves presented, the intensity of the collision seems to be an increasing function of Γ , i.e. the maximum pressure P increases. We understand this as the simple fact that the relative velocity of the collision V_c is increasing with Γ , as it does in this region of Γ in the completely inelastic ball model. What is not possible to explain with this model is the observation that the collision time T_c also seems to be an increasing function of Γ . As discussed before, this is due to the excitation of the internal degrees of freedom of the granular layer, i.e. the layer is dilated.

In Fig. 6 we present the layer density as a function of height for each of the curves introduced in Fig. 5. In general, the density $\rho(z)$ is approximately constant in a center region and decreases toward both ends of the layer. A penetration length for the dilation of the layer can be identified. This length increases with Γ ; for instance, it is of the order of d and $3d$ for $\Gamma \approx 1.4$ and $\Gamma \approx 2.4$ respectively. Another fact that traces back the dilatance of the layer is that its thickness increases with Γ ; it is $14d$ for $\Gamma \approx 1.4$ and $17d$ for $\Gamma \approx 2.8$. In the limit of $\Gamma \sim 1$ we obtain that the density in the central part of the layer is close to ρ_o .

Another interesting piece of information is the bulk dilation within the layer, δ , as a function of z . This quantity is linked directly to the density as $\rho(z) = \bar{v} m_o / (d + \delta)^3$, where \bar{v} is an average coordination number and m_o the particle mass [3]. Defining $\delta = 0$ for $\rho(z) = \rho_o$ we obtain

$$\frac{\delta(z)}{d} = \left(\frac{\rho(z)}{\rho_o} \right)^{-\frac{1}{3}} - 1 \quad (14)$$

Then, it is possible to find $\delta(z)$ for all the data presented previously, which is what is shown in Fig. 7. From this figure, we can qualitatively examine the dependence of $\delta(z)$ on Γ , as we did with $\rho(z)$. For instance, as we increase Γ , the top and the bottom of the layer continuously dilate and the extension of the dilated part increases. The central part also dilates as Γ increases; for $\Gamma \approx 1.4$ and $\Gamma \approx 2.4$ it is of the order of $0.004d$ and $0.02d$ respectively. We also notice that for $\Gamma \approx 2.4$, the value $\delta \approx 0.1d$ is reached for $z \approx 2d$ and $z \approx 15d$, while the total height of the layer is approximately $17d$.

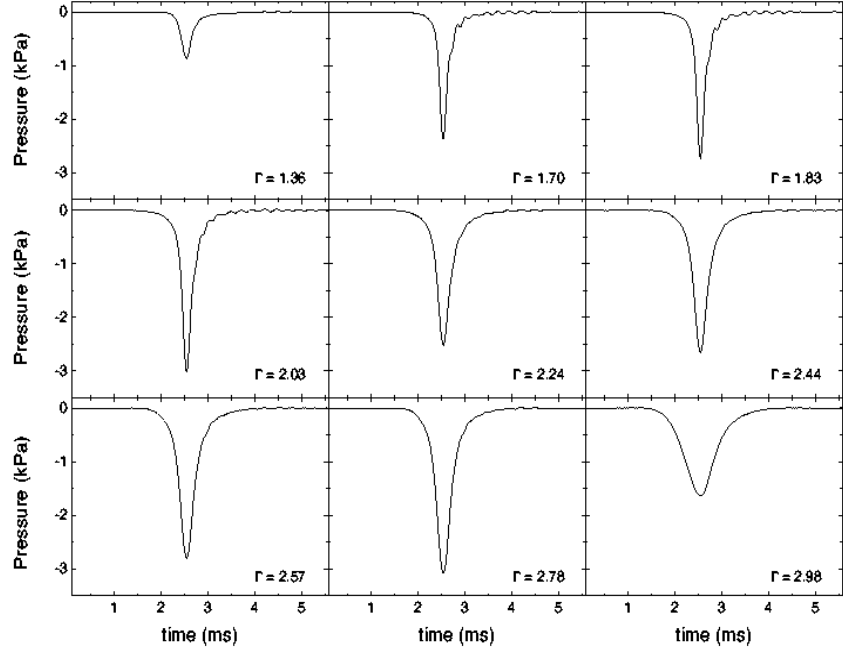


FIG. 5. Averaged pressure peaks as functions of time for various values of Γ and $f = 40$ Hz. For $\Gamma = 2.98$ the layer is already in the wave regime.

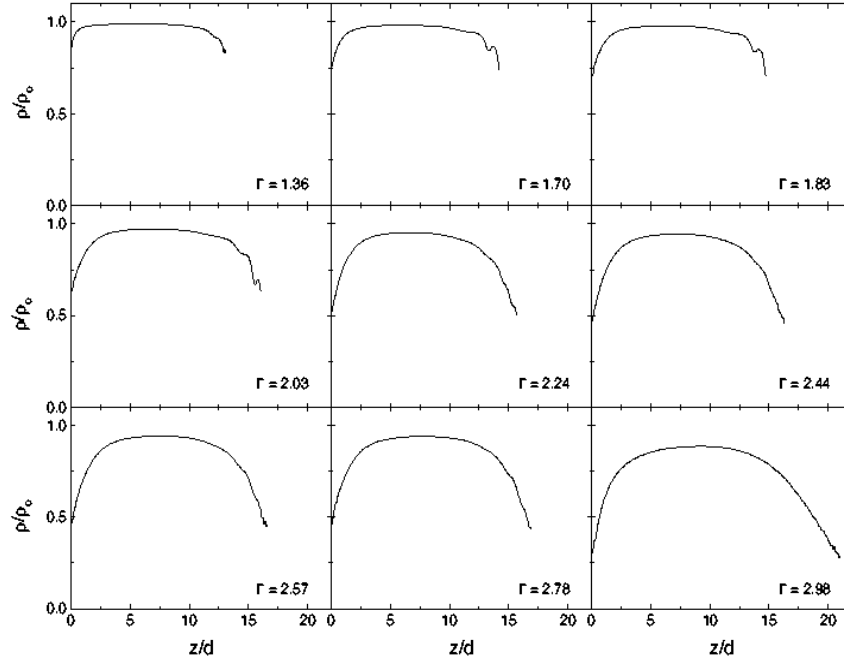


FIG. 6. Normalized density, $\rho(z)/\rho_0$, as function of height, z , for various values of Γ and $f = 40$ Hz.

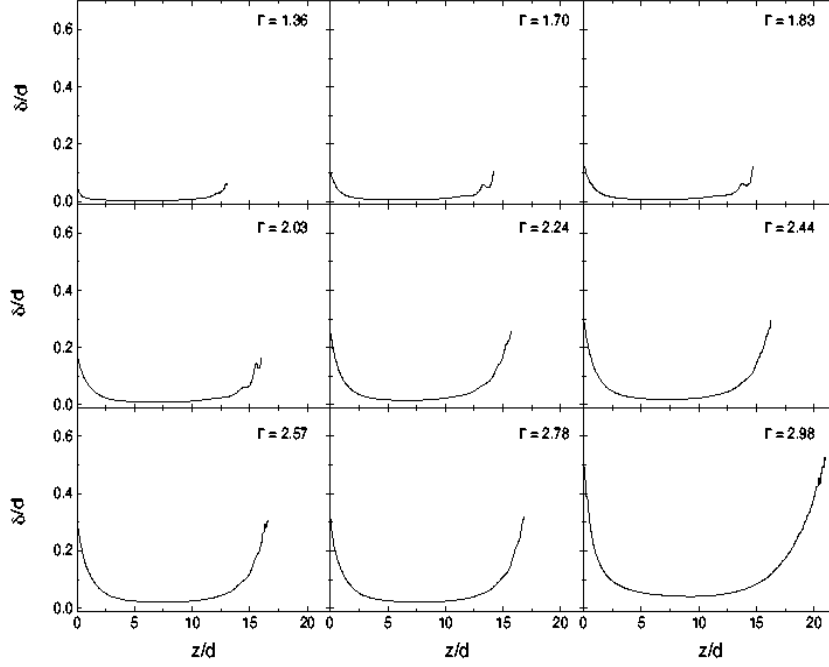


FIG. 7. Normalized dilation, $\delta(z)/d$, as function of height, z , for various values of Γ and $f = 40$ Hz.

At this point, it seems appropriate to define a quantity as the vertical average of $\delta(z)$; we do this because it is necessary to link it in some way to δ_b . Therefore, we define this average dilation as

$$\langle \delta \rangle = \frac{1}{H'} \int_0^{H'} \delta(z) dz \quad (15)$$

where H' is the total height of the layer. Notice that H' depends on the excitation intensity (i.e, it depends on Γ and f).

Fig. 8 presents $\langle \delta \rangle$ versus Γ for several excitation frequencies. We observe in the low frequency regime that $\langle \delta \rangle$ presents a transition at $\Gamma \approx 2$. In contrast, at high f this transition has the tendency to disappear and we observe that $\langle \delta \rangle$ is roughly a linear function of Γ . Complementing the previous data, in the inset of Fig. 8 we present $\langle \delta \rangle$ versus f for two values of Γ , below and above $\Gamma = 2$. The average dilation $\langle \delta \rangle$ is a decreasing function of f . We also present with continuous lines the fits $\langle \delta \rangle \sim f^b$; we find $b = -1.38 \pm 0.06$ and $b = -1.58 \pm 0.03$ for $\Gamma = 1.5$ and $\Gamma = 2.4$ respectively. Similar behaviors are obtained for δ_b , as a function of both Γ and f (See section IV).

To conclude, in this section we have introduced the peak shape of pressure from which we have obtained density profiles. We have discussed these results in a qualitative way and found that dilation is a function of the vertical coordinate. These results, which show that dilation is approximately constant in the bulk but increases sharply close to the free surface of the layer, are similar

to the ones reported in previous works in one and two dimensions [13,14]. We have also shown that at a low frequency of excitation, a critical value of $\Gamma \approx 2$ exists where an abrupt change in the layer dilation takes place. This transition will be discussed in detail in the next section.

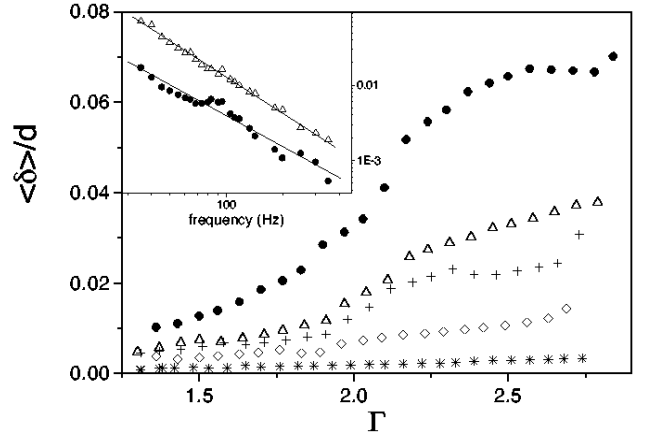


FIG. 8. Average dilation, $\langle \delta \rangle$, versus Γ for various values of f ; (\bullet) $f = 40$ Hz, (Δ) $f = 55$ Hz, ($+$) $f = 70$ Hz, (\diamond) $f = 120$ Hz and ($*$) $f = 250$ Hz. In the inset, log-log plot of $\langle \delta \rangle$ versus f for $\Gamma = 1.5$ (\bullet) and 2.4 (Δ). The continuous lines show the fits $\langle \delta \rangle \sim f^b$ for each Γ , with $b = -1.38 \pm 0.06$ and $b = -1.58 \pm 0.03$ respectively.

IV. PRESSURE AND REFLECTIVITY MEASUREMENTS

Both the time-evolution of the pressure and the intensity are represented in Fig. 9 as a function of Γ when f is in the low frequency regime. For $\Gamma > 1$, the layer-plate collision is always visible in the pressure signal as large peaks. However, no trace of this collision is observed in the reflected light up to $\Gamma \sim 2$. Thus, for $1 < \Gamma < 2$ the layer is compact, indicating that the energy injected during the layer-plate collision is completely dissipated by the multiple collisions between the grains or by friction. In contrast, for $\Gamma > 2$ the time mean value of the reflected light (DC component) exhibits a strong decrease that shows that the layer undergoes a transition from a compact to a dilated state. A modulation in time (AC component) which oscillates at the forcing frequency is also observed in the reflected light for $\Gamma > 2$. This modulation is in phase with the pressure peak. Indeed, immediately after the pressure peak occurs, reflected light increases, indicating that the layer was dilated during the free flight, and that a small compression occurs due to the collision. Furthermore, when the layer takes off, surface dilation starts to increase (a decrease in reflected light).

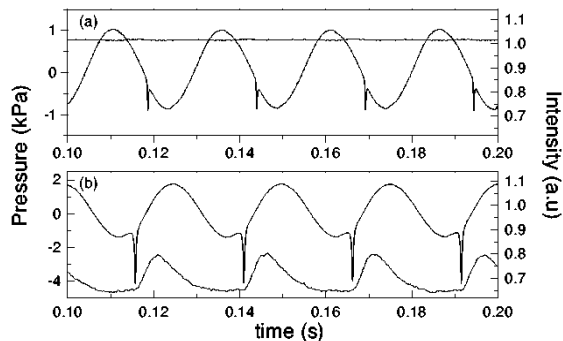


FIG. 9. Time series obtained from pressure and intensity sensors for $f = 40$ Hz; a) $\Gamma = 1.2$, b) $\Gamma = 2.3$.

We first emphasize that this increase in surface dilation is the result of the amplification of small differences in initial conditions, for the free flight of the grains located at the layer surface [15]. Such differences arise as a consequence of the random character of kinetic energy injection; due to the random packing of grains, a layer plate collision naturally induces velocity fluctuations in the layer. As shown in Fig. 9 b for $\Gamma > 2$, the layer never reaches a compact state, which would correspond to a higher value of the reflected light (See Fig. 9 a). This result indicates that kinetic energy, injected into the internal degrees of freedom of the layer, has not been completely dissipated within the cycle. To estimate the amount of energy not dissipated, we consider small changes of I in time for early stages of the layer expansion. We can then write $I(t)/I_{ref} \approx$

$1 - 2\Delta\delta_s(t)/(d + \delta_s(0))$. Here $\Delta\delta_s(t) = \delta_s(t) - \delta_s(0)$ and the reference intensity I_{ref} is taken when the layer starts to expand and corresponds to a finite dilation $\delta_s(0)$ at $t = 0$. From the slope of intensity versus time for early stages of the layer expansion we obtain a characteristic time τ . Dimensionally $\tau^{-1} \sim \Delta V_{to}/(d + \delta_s(0))$, where ΔV_{to} can be associated with the velocity fluctuations at the taking off time of the particles located at the free surface of the layer. Experimentally, τ is close to 1/27 s and is almost independent of frequency. Thus, our estimate shows that $\Delta V_{to}/V_c$ increases linearly with frequency like $2 \times 10^{-4}f$, varying from 0.01 for low f (~ 35 Hz) to 0.04 for intermediate f (~ 200 Hz). Here V_c is the layer-plate relative velocity at the collision calculated from the completely inelastic ball model. Therefore, our results indicate that for $2 < \Gamma < 2.8$, the ratio of residual energy to energy injection, $(\Delta V_{to}/V_c)^2$, increases with f , implying that energy dissipation decreases with f . At this stage, the important feature of typical velocity fluctuations, or “temperature”, at the free surface of the layer arises: we notice that although most of the energy is dissipated, a small amount of residual “thermal energy” is enough to sustain surface dilation.

We focus now on the transition from a compact to a dilated state suffered by the layer at $\Gamma \sim 2$. Fig. 10 illustrates the pressure, P , the collision time, T_c , and the reflected intensity versus Γ for $f = 40$ Hz. P corresponds to the maximum pressure exerted on the plate during the collision and T_c here is defined as the width of the pressure peak at a quarter of its height. We also present in Fig. 10a the numerical fit of P with V_c/T_c ; it is evident that $P \sim V_c/T_c$, which is a natural consequence of the impulsive nature of the periodic forcing. At $\Gamma \sim 2$, the DC component of the intensity exhibits a strong decrease while its AC component abruptly increases. At the same value of Γ there is a small decrease in the pressure peak, and a small increase in T_c , due to an increase in the bulk dilation in the layer. This decrease in pressure was already observed by P. Umbanhowar [8], and it is stronger for particles with higher restitution coefficients; however, no correlation with reflectivity measurements were made to investigate the state of the layer. We emphasize that the former transition occurs for $\Gamma < \Gamma_w$. At the onset of surface waves ($\Gamma = \Gamma_w$), the pressure presents a strong decrease associated with the fact that layer-plate collision is spread out in time [8] (Fig. 10 a, b).

Using the considerations introduced in the previous section, we calculate δ_b and δ_s as functions of Γ . This is presented in Fig. 11 for $f = 40$ Hz. To complete the data, we also present the average dilation $\langle \delta \rangle$, and we observe that the agreement with δ_b is fairly good. Similar to what we found for $\langle \delta \rangle$ (fig. 8), we observe that both δ_b and δ_s suffer transitions at $\Gamma \approx 2$. Curiously, for $\Gamma < 2$ the bulk dilation is higher than the dilation in surface and δ_s takes negative values, which simply means that the layer surface reaches a state more compact than the initial one. This is related to the fact that the initial state, consistent with our experimental method [7],

is not the more compact accessible state of the layer. Therefore we say that for $\Gamma < 2$ the state of the layer is solid-like, where the injected energy during the collision is completely dissipated. However, in this regime, the available energy is enough to produce rearrangement of surface grains. In all the cases tested, the maximum compaction was never larger than 2% of the initial density. Consequently, we associate the increase in δ_s and δ_b , observed at low f and $\Gamma > 2$ to a solid-liquid type transition. In the liquid phase, average dilation is large enough to allow particles to move with respect to each other. For low f , at the critical value $\Gamma \approx 2$, the injected energy rate becomes larger than the dissipation rate, and the energy excess sustains the dilation in the granular layer.

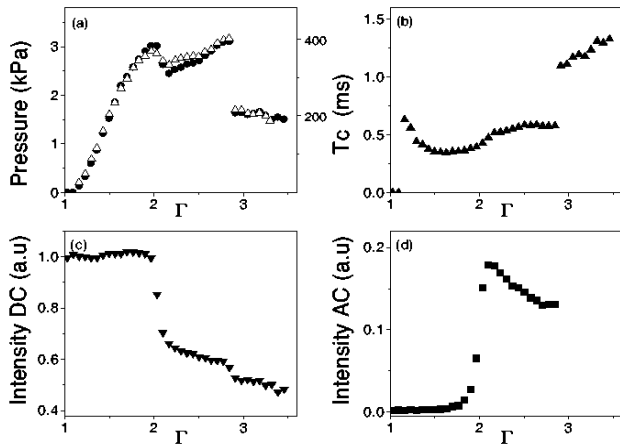


FIG. 10. Maximum pressure P , collision time T_c , DC and AC components of intensity versus Γ for $f = 40$ Hz. In (a) we present the fitting of the maximum pressure P (\bullet) with V_c/T_c (Δ), whose magnitude is presented in the right axis in units of m/s^2 .

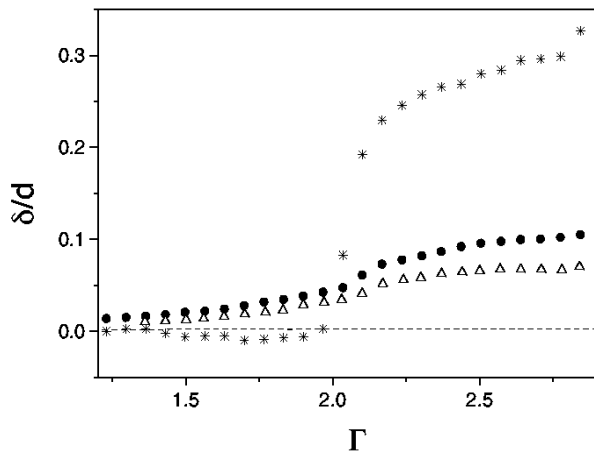


FIG. 11. Bulk dilation, δ_b (\bullet), mean dilation, $\langle\delta\rangle$ (Δ), and surface dilation, δ_s (*), versus Γ for $f = 40$ Hz.

In Fig. 12 we include frequency dependence of the same

quantities presented in Fig. 10. As opposed to the case of low f , at high f and for $\Gamma > 2$ the DC component of I increases slightly. This indicates that the layer surface has reached a state more compact than the initial one. It is very important to notice that the decrease in pressure associated with the wave instability is clearly observed over the entire range of frequencies (Fig. 12 a). Complementing Fig. 12, we present in Fig. 13 a and c the maximum pressure and the DC component of intensity versus f for two values of Γ , both smaller than the critical one for waves, with one right below and the other right above the fluidization transition. Both the maximum pressure and the jump in reflectivity decrease as f increases.

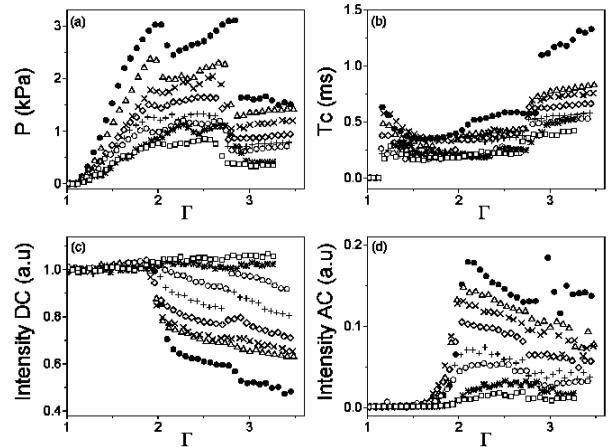


FIG. 12. Maximum pressure, P , collision time, T_c , and DC and AC components of intensity versus Γ for various f ; $f = 40$ (\bullet), 69 (Δ), 83 (\times), 111 (\diamond), 154 ($+$), 200 (\circ), 250 ($*$) and 350 (\square) Hz.

We also present the bulk dilation δ_b (See Fig. 13 b) calculated directly from the pressure through equation (2). We find that δ_b scales as f^b with $b = -1.42 \pm 0.07$ and $b = -1.54 \pm 0.03$ for $\Gamma = 1.5$ and 2.3 respectively. These values are in very good agreement with those obtained for $\langle\delta\rangle$ (See Fig. 8), and they provide a consistency test for both kinds of measurements. These results indicate that the relevant quantity is not only the ratio of the injected energy per particle to the potential energy required to rise a particle by a fraction of its diameter, in which case δ_b would vary as $1/f^2$, but also the dissipated energy. We notice that our results contrast with those obtained by Luding *et al* in numerical simulations of a column of particles in the completely fluidized regime, where the average dilation scales as $\langle\delta\rangle \sim (Af)^2$, which for Γ constant becomes $\langle\delta\rangle \sim (\Gamma/f)^2$ [13]. However, similar simulations done by the same group for a two-dimensional layer [16] indicate that the layer expansion scales as $h_{cm} - h_{cmo} \sim (Af)^{3/2} \sim (\Gamma/f)^{3/2}$. Even though these results were also obtained in a completely fluidized regime (typically $\Gamma > 10$) we observe quite good agreement for the *scaling on f* for the expansion of the

layer.

On the other hand, information about the surface dilation, δ_s , versus f is obtained using the intensity data as $I/I_0 \approx d^2/(d + \delta_s)^2$ (See Fig. 13 d). For $f > 225$ Hz, δ_s takes negative values, which indicates that the surface layer is more compact than the initial one [7]. However, in this regime, as shown in the previous section, the bulk dilation increases with Γ but remains very small, $\delta/d \sim 10^{-3}$.

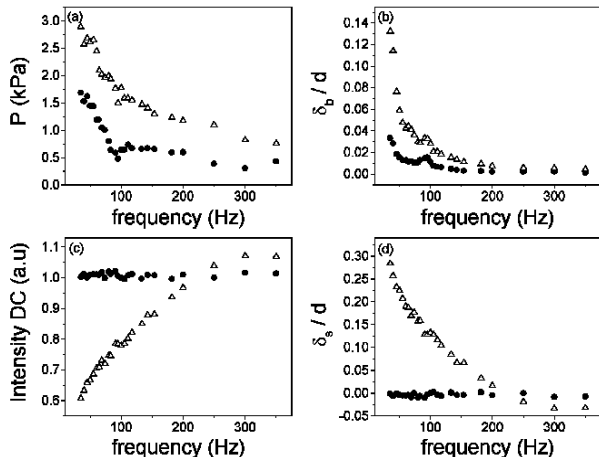


FIG. 13. Maximum pressure P , bulk dilation δ_b , DC component of intensity and surface dilation δ_s versus f for two constant values of Γ below the onset of surface waves; $\Gamma = 1.5$ (\bullet), 2.3 (\triangle). Bulk dilation scales as $\delta_b \sim f^b$ with $b = -1.42 \pm 0.07$ (\bullet) and $b = -1.54 \pm 0.03$ (\triangle) respectively.

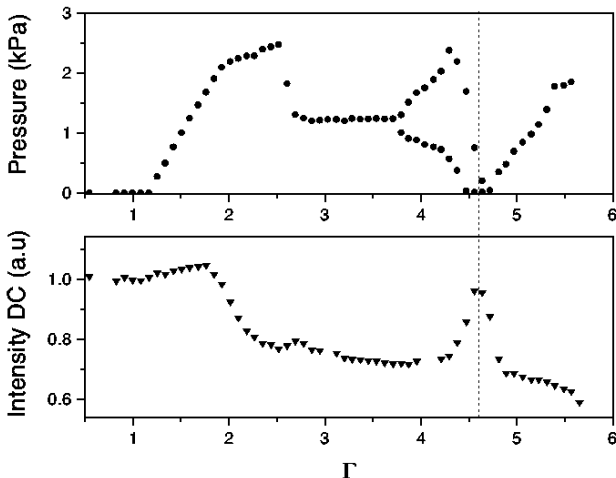


FIG. 14. Maximum pressure P (a) and DC reflectivity-component (b) as a function of Γ for $f = 60$ Hz. The vertical line indicates the flat layer with kinks transition at which $V_c = 0$. At $\Gamma = 3.6$, as predicted by the inelastic colliding ball model for the center of mass of the layer, a period doubling instability is observed.

Finally, let us mention another interesting transition which links to the flat with kinks instability reported in previous works [2]. If we increase Γ further we find that a period doubling is achieved at $\Gamma \approx 3.6$, as reported before [17,2]. Next, for $\Gamma \approx 4.6$, an inverse transition of the liquid-solid type is detected. Fig. 14 shows a typical measurement of both reflected intensity and maximum pressure for a wider range of Γ . We detect that at $\Gamma \approx 4.6$, P strongly decreases and the mean value of intensity strongly increases. Using the results discussed previously, both changes reflect a strong decrease of grain mobility. We notice that the critical value $\Gamma \approx 4.6$ corresponds to $V_c = 0$ in the completely inelastic ball model, so in fact no energy is injected to the internal degrees of freedom. We also conclude that no surface waves can be sustained in this regime, except at the kink itself. Indeed, the shear induced at the kink by the flat parts oscillating out of phase is large and enough to induce dilation. At low frequencies, this dilation is enough to allow hydrodynamics waves, as those shown in figure 1c. As Γ is increased further, the pressure increases and the reflectivity decreases. Thus, energy injection again becomes enough to sustain surface waves in the layer. This fact is consistent with the existence of $f/4$ waves reported previously [2]. Notice that for $\Gamma = 4.6$ the maximum velocity of the plate is $Aw \approx 12$ cm/s; this confirms that the relevant scale of velocity fluctuations is given by V_c and not Aw .

The experimental results presented above can be summarized as follows. Depending on the excitation frequency we observe different kind of states and waves. At low frequency, bulk and surface dilation present strong increases which are associated with a fluidization transition. Surface waves observed in this regime involve large relative motion between particles and are therefore considered as the hydrodynamic modes of the layer. At intermediate f , although the injected energy is small, we still observe a decrease in reflectivity as a function of Γ . In this regime, as shown in Fig. 13 b, δ_b is too small ($\delta_b/d < 0.1$) to allow motion between the particles [18]. Therefore, at the critical Γ , the decrease of reflectivity is the signature of particles fluctuating around their positions at the free surface of the layer. We associate this decrease with a heating up of the solid phase. For higher frequencies, the layer undergoes a compaction transition which is detected by the increase in surface density. Below and above this transition the local bulk dilation δ_b/d is even smaller and is of order 0.005, implying that the mobility in both the bulk and the free surface is completely suppressed. Thus, very low amplitude surface waves detected in the compaction regime, by the strong decrease in the maximum pressure, must correspond to excitations in which the layer is slightly modulated in time and space. We will see in the following section that these waves are bending waves, associated with the ability of the compact layer to deform. Finally, fig. 15 presents the phase diagram for the granular layer: phase boundaries separating the various states and sur-

face waves have been obtained from the data in Fig. 12. The layer state and surface wave transitions occur for approximately constant values of Γ independent of f .

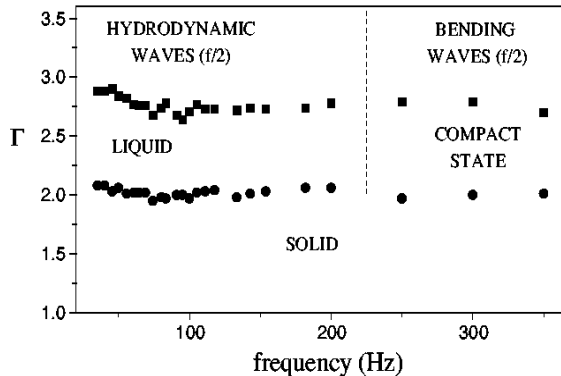


FIG. 15. Phase diagram showing layer state and surface wave transitions. The vertical dashed line at $f = 225$ Hz defines the frequency above which the layer strictly undergoes a transition to a state more compact at $\Gamma \sim 2$.

V. LOW AMPLITUDE WAVES: BENDING WAVES

To check the existence of these waves we have performed a set of experiments in a two-dimensional granular layer. The advantage of using a two-dimensional system is that this allows us to obtain side views of the waves. This is of particular importance since bending waves are difficult to visualize as they have amplitudes of the order of fifty percent of a particle diameter.

In order to observe such small amplitudes we have used photoelastic cylinders of 6 mm in diameter and 6.35 mm in length. Typical excitation frequencies are about 40 Hz, which for this system are in the high frequency regime. We recall that this regime occurs for frequencies much larger than the frequency crossover, $f \sim \sqrt{g/d}$. When varying the deepness of the layer (number of particles = N), this scaling becomes $f \sim \sqrt{g/Nd}$ [19]. In the case of bronze particles of $d \approx 0.12$ mm, bending waves are detected for $f > 225$ Hz. This tells us that these waves should be observed at $f \approx 40$ Hz, for $d = 6$ mm and a layer about ten particle diameters thick. With these parameters, for $\Gamma \sim 3.5$, the amplitude of waves should be of the order of 1 mm.

Typical snapshots of two stages of bending waves at $\Gamma = 3.5$, $f = 40$ Hz and $N = 10$ are presented in figures 16a and 16b. We observe that the layer slightly bends with respect to the horizontal. Similar to what occurs for low frequency waves, this modulation alternates in time at half of the frequency forcing (See below). However, in this case, the wavelength of the modulation is about a layer thickness and is also nearly independent of f . Some particles are marked with black spots which allows us to distinguish them and follow their trajectory

(See Fig. 16a, b). As expected, the mobility of the particles is very low. Only at the surface layer will some particles move with respect to each other over distances of the order of the driving amplitude. In the bulk this motion is completely suppressed.

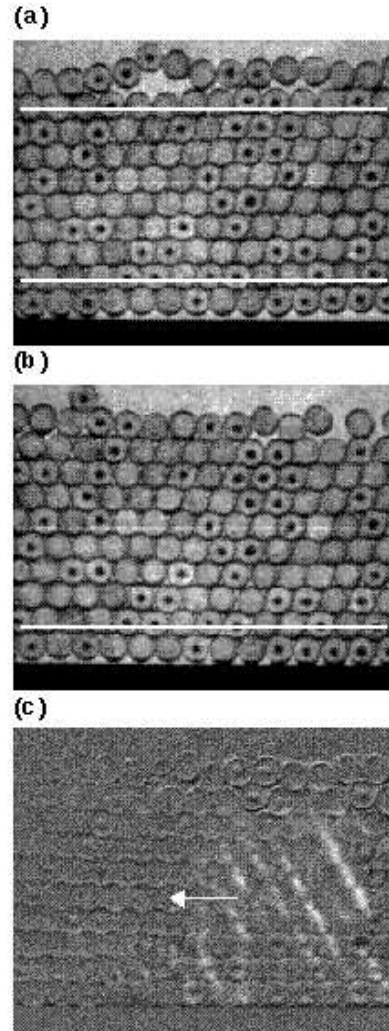


FIG. 16. Typical snapshots of bending waves for $f = 40$ Hz and $\Gamma = 3.6$. In (a) and (b) the white horizontal lines show that the layer bends itself about half a diameter. Both states alternate in time with the frequency of oscillation. In (c) we present the difference of two images during a collision. The bright zones correspond to regions under high stress. In this case the compression front travels to the left.

Additional support for these low amplitude waves is provided in Fig. 16c in which a compaction front that moves laterally is observed as a bright zone. This image results from the difference of two consecutive snapshots (period of acquisition is about 0.8 ms). At a compression zone, the vertical stress in the layer is high so the light is transmitted. Thus, the difference of images mainly shows the zones under stress. In the case presented the com-

pression front moves from right to left and the collision occurs very near the right boundary of the image. In the next cycle the collision occurs near the left boundary and the compression front travels to the right. With a wider view of the layer we observe that in fact two compression fronts are created from each collision point; one front travels in each direction. This kind of visualization allows us to safely say that these parametric waves are also subharmonic, i.e. their frequency is $f/2$. Finally, from the images we estimate the velocity of the compression front of the order of a few meters per second. This value is very high compared to the estimated velocity at the collision $V_c \approx 0.25$ m/s; this indicates the existence of contact arcs (see the contact lines in Fig. 16c) so the layer is almost not dilated.

VI. CONCLUSIONS

In conclusion, depending on the excitation frequency, we observe different kinds of states and waves. Thus, our experimental results reveal the existence of a solid-liquid transition that precedes subharmonic wave instability. Hydrodynamic surface waves can be then considered as the natural excitations existing in a fluidized granular layer. In contrast, very low amplitude surface waves detected in the compaction regime correspond to excitations in which the layer slightly bends alternatively in time and space. We have seen in the previous section that these waves are associated with the compact character of the layer. The layer states observed here and surface wave transitions occur for approximately constant values of Γ independent on f .

Additional experimental evidence of the fluidization transition experienced by the layer at $\Gamma \sim 2$ can be found in reference [20] (See for instance, Fig. 6 in ref. [20]). Although they used rather large particles at small forcing frequencies, we find that their experiments are actually in the low frequency regime after estimating the frequency crossover. Independent experimental evidence for the compaction transition is also found in previous works. For instance, a strong increase in granular density was found, close to $\Gamma \sim 1.9$, in several experiments on large columns of grains submitted to “taps” of a single cycle of vibration [21]. In this case, applying the scaling to the frequency crossover, we found consistently that these experiments correspond to the high frequency limit. Therefore, we conclude that both fluidization as well as compaction transitions are well established experimentally. However, it is still unclear what mechanisms dominate these transitions and why they arise at a constant value of Γ . We can only safely say that at low energy injection rates, or equivalently at small plate amplitudes with respect to the thickness of the layer, the transition will be of the compaction type. In the opposite case of high energy injections rates, this transition will be of the fluidization type.

Also, we have clearly shown that the relevant scale of velocity fluctuations is given by V_c and not Aw . Then, via the intensity measurements we deduced that the dissipation decreases as f is increased; this is equivalent to state that the dissipative effects increase with velocity fluctuations. A possible cause of this is the dependence on the velocity of the restitution coefficient: it has been recently shown that $1 - \epsilon \sim v^\alpha$, where v is the relative normal velocity at the collision and α a positive number [22]. Nevertheless, as the dilation is reduced we expect that the friction between grains will become an important dissipative mechanism.

Finally, the importance of the bulk and surface dilation measurements is that they provide a complementary way, with respect to the granular temperature, to explore the excitation of the internal degrees of freedom of a vibrated layer. For the dilation in the bulk we have found that, for a constant value of Γ , it is a decreasing function of f of the form $1/f^b$, with $b \approx 3/2$. This agrees with previous simulations of a two dimensional layer [16]. It is clear that the deviation from the expected value $b = 2$ is due to dissipative effects, but the exact numerical value seems to depend on Γ .

It is a pleasure to acknowledge to Paul Umbanhowar and Enrique Tirapegui for many enlightening discussions and to Satish Kumar for useful comments on the manuscript. This work was supported by Fondecyt Grant N01970682, Catedra Presidencial en Ciencias and Dicyt USACH.

-
- [1] For recent reviews, see H.M Jaeger, S.R. Nagel, and R.P. Behringer, *Phys. Today* **49**, No 4, 32 (1996); *Rev. Mod. Phys.* **68**, 1259 (1996).
 - [2] F. Melo, P. Umbanhowar and H. L. Swinney, *Phys. Rev. Lett.* **72**, 172 (1994). F. Melo, P. Umbanhowar and H. L. Swinney, *Phys. Rev. Lett.* **75**, 3838 (1995).
 - [3] It is well known that the mobility in a granular material depends strongly on the energy injection rate. See for instance P. K. Haff, *J. Fluid Mech.* **134**, 401 (1983).
 - [4] P. Umbanhowar, F. Melo and H. L. Swinney. *Nature* **382**, 793 (1996).
 - [5] N. Mujica and F. Melo, *Phys. Rev. Lett.* **80** 5121 (1998).
 - [6] H.K. Pak, E. Van Doorn, and R.P. Behringer, *Phys. Rev. Lett.* **74**, 4643 (1995).
 - [7] I_0 is obtained after a “fluidization” of the layer, for many cycles, at $\Gamma = 2.4$ and $f = 40$ Hz. Before each measurement we set the initial state of the layer by this procedure.
 - [8] P. Umbanhowar, Ph.D. Thesis, University of Texas at Austin, (1996). P. Umbanhowar, F. Melo and H. L. Swinney, (unpublished).
 - [9] E. Falcon, C. Laroche, S. Fauve and C. Coste, *Eur. Phys. J. B* **5**, 111 (1998).
 - [10] L.D. Landau and E.M. Lifshitz, Section 9, *Theory of*

- Elasticity*, 3rd Edition, Pergamon Press (1986).
- [11] Both times T_q and τ_1 depend on the velocity of collision as $V_c^{-1/5}$ and the estimates in the text correspond to the lowest values of V_c achieved in our experiments.
- [12] A. Goldshtein, M. Shapiro and C. Gutfinger, *J. Fluid. Mech.* **316**, 29 (1996).
- [13] S. Luding, E. Clement, A. Blumen, J. Rajchenbach, and J. Duran, *Phys. Rev. E*, **49**, 1634 (1994).
- [14] E. Clement and J. Rajchenbach, *Europhys. Lett.*, **16**, 139 (1991), J.A.C Gallas, H. Herrmann, and S. Sokolowski, *Physica (Amsterdam)* **189A**, 437 (1992).
- [15] Simple numerical simulations show that the experimental variation of intensity, during the free flight of the layer, is reproduced by assuming small velocity fluctuations at the take off time for the particles located at the free surface. Such velocity fluctuations are very close to the ones estimated in the text. N. Mujica and F. Melo, (unpublished).
- [16] S. Luding, H. Herrmann and A. Blumen, *Phys. Rev. E* **50**, 3100 (1994).
- [17] S. Douady, S. Fauve and C. Laroche, *Europhys. Lett.* **8**, 621 (1989).
- [18] O. Reynolds, *Philos. Mag. Ser. 5*, **20**, 469 (1885).
- [19] C. Bizon, M.D. Shattuck, J.B. Swift, W.D. McCormick and H. Swinney, *Phys. Rev. Lett.* **80** 57 (1998).
- [20] C.E. Brennen, S. Ghosh and C.R. Wassgren, *J. Appl. Mech.* **63**, 156 (1996).
- [21] J. B. Knight, C. G. Fandrich, Chun Ning Lau, H. M. Jaeger, and S. R. Nagel, *Phys. Rev. E* **51**, 3957 (1995).
- [22] E. Falcon, C. Laroche, S. Fauve and C. Coste, *Eur. Phys. J. B.* **3**, 45 (1998).